pISSN 1229-3008 eISSN 2287-6251
Progress in Superconductivity and Cryogenics
Vol.25, No.4, (2023), pp.75~80 https://doi.org/10.9714/psac.2023.25.4.075

# Discretized solenoid design of a 1.5 T and a 3.0 T REBCO whole-body MRI magnets with cost comparison according to magnetic flux

**Wonju Jung, Geonyoung Kim, Kibum Choi, Hyunsoo Park, and Seungyong Hahn***

*Department of Electrical and Computer Engineering, Seoul National University, Seoul, Korea*

(Received 23 November 2023; revised or reviewed 28 December 2023; accepted 29 December 2023)

**Abstract**

Rare earth barium copper oxide (REBCO) materials have shown the possibility of high-temperature superconductor (HTS) magnetic resonance imaging (MRI) magnets due to their elevated transition temperature. While numerous MRI magnet designs have emerged, there is a growing emphasis on estimating the cost before manufacturing. In this paper, we propose two designs of REBCO whole-body MRI magnets: (1) 1.5 T and (2) 3.0 T, the standard center field choices for hospital use, and compare their costs based on conductor usage. The basis topology of the design method is based on discretized solenoids to enhance field homogeneity. Magnetic stress calculation is done to further prove the mechanical feasibility of their construction. Multi-width winding technique and outer notch structure are used to improve critical current characteristic. We apply consistent constraints for current margins, sizes, and field homogeneities to ensure an equal cost comparison. A graph is plotted to show the cost increase with magnetic flux growth. Additionally, we compare our designs to two additional MRI magnet designs from other publications with respect to the cost and magnetic flux, and present the linear relationship between them.

*Keywords*: MRI magnet, MRI cost, REBCO

## 1. INTRODUCTION

Magnetic resonance imaging (MRI) is a valuable tool for diagnosing medical conditions by visualizing internal body structures. Traditional MRI magnets are constructed using low-temperature superconductors (LTS), despite the discovery of high-temperature superconductors (HTS) [1-5]. HTS has a key selling point which is the 'high critical temperature' compared to LTS but due to its practical problems including the high cost, it is still challenging to build an MRI magnet with HTS.

Rare earth barium copper oxide (REBCO) is a type of high-temperature superconducting (HTS) material that has been developed for use in various industries and medical applications, including MRI magnets. The cost of REBCO superconducting tapes varies between manufacturers and is generally significantly higher than low-temperature superconducting (LTS) wires [6-8]. Despite the cost challenge, some laboratories have constructed HTS MRI magnets for research purposes [9-12].

Higher critical magnetic field of REBCO makes it essential for high-field MRI magnet designs [13]. However, the magnet cost takes the largest portion of an MRI system, underscoring the importance for magnet engineers to create cost-effective designs for MRI magnets. This is essential for ensuring competitiveness with conventional LTS MRI magnets [14-15].

While numerous studies have explored the design aspects of MRI magnets, our work explicitly focuses on the economic implications of magnet development. The originality of our research lies in the comprehensive comparison of the conductor costs associated with our designed 1.5 T and 3.0 T magnets against existing magnet designs. This approach offers valuable insights into the economic feasibility and potential cost efficiencies in magnet design and construction.

In this paper, we present two designs for REBCO whole-body MRI magnets one for 1.5 T and the other for 3.0 T with comparing their conductor costs depending on their magnetic flux including two more designed MRI magnets in other papers. MRI magnets are divided into three pairs of solenoid coils for the field homogeneity optimization and outer notches are implemented to improve the critical current distribution. The mechanical feasibility of the designs is shown by calculating the magnetic stress.

## 2. MAGNET DESIGN METHOD

### 2.1. Conductor specification

We chose SuperOx as the manufacturer for the REBCO conductor used in our design. The tape widths ranged from 4.1 mm to 7.1 mm for the multi-width winding technique [16]. The thickness of the tape was 0.075 mm.

### 2.2. Design specification

The main coil's inner winding radius was set at 450 mm to accommodate an average individual with a 40 cm shoulder width inside the bore [17]. This design accounted for the inclusion of additional components, such as gradient and shim coils [18]. Spacers between single pancake (SP) coils and double pancake (DP) coils had a thickness of 0.2 mm. Aim load line current margin was 20%. In MRI applications, achieving a field homogeneity

* Corresponding author: hahnsy@snu.ac.kr

below 1 ppm over the DSV after shimming is crucial for imaging quality. However, immediate post-manufacturing levels have a field homogeneity around 100 ppm. Moreover, since the average shoulder width of men is around 40 cm, the magnetic field should be homogeneous over 40 cm for clear images of the entire body of an individual [19]. Therefore, the target field homogeneity was below 100 ppm over a 40 cm diameter spherical volume (DSV) [20].

### 2.3. Field homogeneity optimization

An ideal, infinitely long solenoid magnet has perfectly homogeneous magnetic fields within, but practical magnets require adjustments to enhance field homogeneity. In order to meet the homogeneity specification, we selected a discretized solenoid structure. This method included modifying the distances between each solenoid pair to minimize field inhomogeneity within predefined height limits. The main coil comprised three pairs of solenoid coils, while the shield coil had one pair, as visually represented in the scaled illustration provided in Fig. 1.

The field homogeneity, which was the objective function, was calculated by the equation below:

$$\frac{\Delta B}{B} = \frac{B_{max} - B_{min}}{B_{max} + B_{min}}, \quad (1)$$

where $B_{max}$ and $B_{min}$ are maximum and minimum magnetic fields within 40 cm DSV. We optimized the axial placement of the solenoid pairs to achieve the best field homogeneity within the specified height limits. If the optimal homogeneity exceeded 100 ppm, we relaxed the limit and extended the magnet length, aiming to achieve homogeneity below 100 ppm. Fig. 1 shows how we set the optimization variables. M1 and M2 shared an identical length, shorter than M3, due to the coils nearer to the magnet center contributing to higher field inhomogeneity. This division simplified the homogeneity optimization process.

For the shield coil, the winding inner radius was fixed at double that of the main coil, enabling us to identify a suitable point where it could reduce the 5 G line without significantly affecting the center field. The location of the shield coil remained a constant, unaltered during optimization iterations, simplifying the overall process. The axial maximum location of the shield coil was consistently set to the height limit throughout different optimization round runs.

### 2.4. Critical current optimization

The critical current of a REBCO tape is influenced by the external magnetic field, particularly the magnetic field magnitude and angle. These two parameters determine the critical current at a specific temperature. In a solenoid magnet, the magnetic field exhibits similar values within the winding bore, with the field angle being the dominant factor that determines the critical current.

When the magnetic field is perpendicular to the REBCO tape surface, the critical current is at its lowest. On the other hand, the critical current is highest when the field is

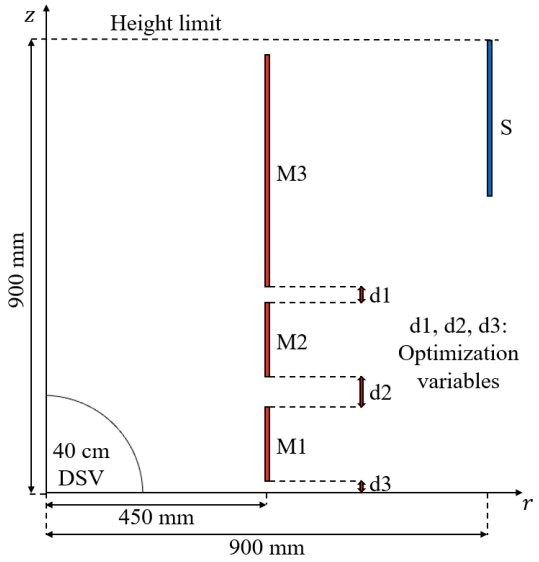


Fig. 1. A scaled quadrant cross-sectional illustration of the magnet design method. M1, M2, and M3 represent the discretized solenoid pairs for the main coil while S corresponds to the shield coil. Distances between the pairs are denoted as d1, d2, and d3 which were optimization variables.

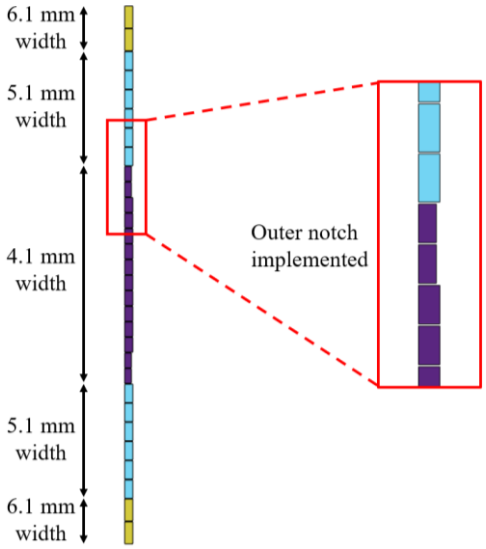


Fig. 2. A scaled cross-sectional view of M1 (only 3.0 T case is shown). The outer notch is enlarged to show the difference between the turns with and without the notch.

parallel to the tape surface. Based on this understanding, we can intuitively deduce that the critical current of the coils located at the edges of a solenoid magnet is lower than that of the inner coils due to the larger radial magnetic field. Consequently, we positioned REBCO tapes with larger widths at the edges of each discretized solenoid pair.

As the tape width increases, the current density decreases, resulting in a smaller axial magnetic field. The remaining magnetic flux contributes to an increase in the radial magnetic field. Consequently, the critical currents are lower at the transition points where tape width changes.

In the MRI magnet design, there were three distinct transition points: from 4.1 mm to 5.1 mm, from 5.1 mm to

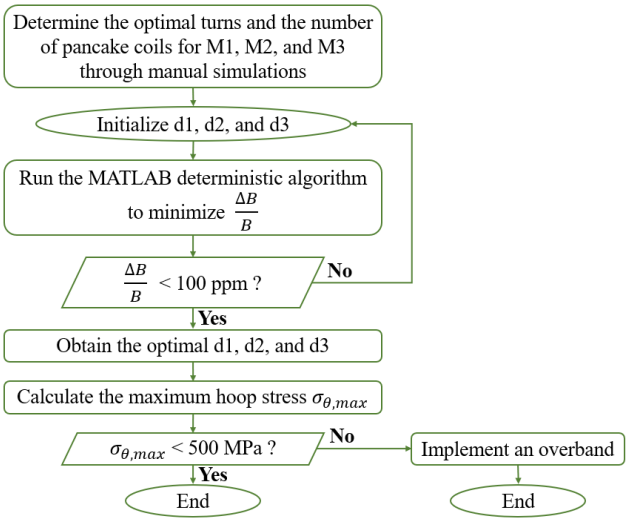


Fig. 3. Flow chart of the MRI magnet design process.

6.1 mm, and from 6.1 mm to 7.1 mm. Among these, the transition from 4.1 mm to 5.1 mm represents the most significant change in width. To deal with this, we reduced the number of turns in the coil with 4.1 mm tape at the transition point, implementing so called the notch structure. This allowed the axial magnetic field to gradually decrease, resulting in higher critical currents compared to the magnet design without the notches. We removed the turns from the outside and these outer notches are shown in Fig. 2. The overall design flow chart is shown in Fig. 3.

## 3. DESIGN RESULTS

### 3.1. Coil dimension

For the 1.5 T MRI magnet, we used 12 turns of REBCO tape in each single pancake for the main coil, with 8 turns in the shield coil. The optimized d1, d2, and d3 were 27.02 mm, 61.57 mm, and 31.97 mm, respectively. The overall height of the magnet was 1750 mm, with 19.2 km of conductor usage in a 4.1 mm equivalent length.

In the case of the 3.0 T MRI magnet, we increased the number of turns to 30 for the main coil and 19 turns for the shield coil. The optimized d1, d2, and d3 were 27.86 mm, 63.27 mm, and 32.39 mm, respectively. The overall height of the magnet reached 1780 mm, and we utilized 46.1 km of conductor in a 4.1 mm equivalent length.

### 3.2. Magnet operation

The design for the 1.5 T MRI magnet was carried out at 20 K, assuming conduction cooling. It operated at 841.9 A. The feasibility of high current operation in a conduction-cooled magnet was demonstrated in [21]. This design had a 21% current margin, and it achieved a field homogeneity of 93.5 ppm over a 40 cm DSV. Fig. 4 was drawn to verify the result of the calculation.

Similarly, the 3.0 T MRI magnet was designed to operate at 20 K using conduction cooling, with an operating current of 675.8 A. It also had a 20% current margin. Over a 40 cm DSV, the field homogeneity reached 88.1 ppm.

### 3.3. Stress analysis

It is important to note that magnetic stress increases with higher magnetic field and current density within the wire. Therefore, we focused our stress analysis on the M1 position, which is the closest to the magnet center and specifically a pancake with a tape width of 4.1 mm, as it exhibits the highest current density.

Our design goal was to create a magnet with full radial compressive stress and hoop stress below 500 MPa, as described in [22-24]. The mechanical properties of the coil winding materials used for the magnetic stress calculation can be found in Table I [25]. We made the assumption of plane stress, neglecting axial force, shear stress, and thermal stress.

To describe the force balance between Lorentz force and internal stress, we used the equation:

$$\frac{\partial \sigma_r}{\partial r} + \frac{\sigma_r - \sigma_\theta}{r} = -JB_z(r,z). \quad (2)$$

Here, $r$, $\sigma_r$, $\sigma_\theta$, $J$ and $B_z$ represent the radial coordinate, radial stress, hoop stress, current density, and the z-component of the magnetic field, respectively [26]. The $B_z(r,z)$ value in equation (2) was assumed to be linear within the coil winding.

The result of the magnetic hoop stress calculation is illustrated in Fig. 5, showing that the hoop stress level met our predefined constraint. Additionally, the radial stress was calculated to be fully compressive.

In the 3.0 T case, the radial stress remained fully compressive, but the calculated hoop stress was 661 MPa. In order to mitigate the hoop stress, we introduced a stainless steel overband. Metal tape co-winding can also reduce hoop stress by lowering current density. However, we chose to implement an overband to reduce the use of REBCO tape and ensure cost-effectiveness.

We used a total overband thickness of 1.5 mm to meet the hoop stress limit. This resulted in a reduction of the maximum hoop stress at the coil winding to 360 MPa, and the maximum hoop stress at the overband was 452 MPa. Both values satisfied the hoop stress constraint.

### 3.4. Cost comparison of MRI magnets

The design process aimed to create two MRI magnets with different center fields but similar dimensions to facilitate cost comparison, where cost was evaluated based on the length of REBCO tape used in each magnet.

TABLE I
MECHANICAL PROPERTIES OF THE REBCO TAPE AND THE OVERBAND.

| Parameters | Units | Values |
|---|---|---|
| REBCO | | |
| Equivalent Young's modulus ($E_r$, $E_\theta$) | [GPa] | 100; 150 |
| Equivalent Poisson's ratio ($\nu_{r\theta}$) | | 0.18 |
| Yield strength | [MPa] | 500 |
| Stainless steel overband | | |
| Equivalent Young's modulus ($E_r$, $E_\theta$) | [GPa] | 190; 190 |
| Equivalent Poisson's ratio ($\nu_{r\theta}$) | | 0.30 |
| Yield strength | [MPa] | 500 |

TABLE II
COIL DIMENSION PARAMETERS OF THE MRI MAGNETS.

| Parameters | Units | 1.5 T | 3.0 T |
|---|---|---|---|
| Main coil winding inner radius | [mm] | 450.00 | |
| Main coil winding outer radius | [mm] | 450.90 | 452.25 |
| Turns per main coil SP | | 12 | 30 |
| Shield coil winding inner radius | [mm] | 900.00 | |
| Shield coil winding outer radius | [mm] | 900.60 | 901.42 |
| Turns per shield coil SP | | 8 | 19 |
| SP-SP spacer thickness | [mm] | 0.2 | |
| DP-DP spacer thickness | [mm] | 0.2 | |
| Total number of DP coils | | 208 | 210 |
| d1 | [mm] | 27.02 | 27.86 |
| d2 | [mm] | 61.57 | 63.27 |
| d3 | [mm] | 31.97 | 32.39 |
| Overall height | [mm] | 1750 | 1780 |
| Total conductor usage (4.1 mm equivalent) | [km] | 19.2 | 46.1 |

TABLE III
OPERATION PARAMETERS OF THE MRI MAGNETS.

| Parameters | Units | 1.5 T | 3.0 T |
|---|---|---|---|
| Center field | [T] | 1.5 | 3.0 |
| Operating temperature | [K] | 20 | |
| Operating current | [A] | 841.9 | 675.8 |
| Critical current at the load line | [A] | 1062 | 849.7 |
| Current margin | [%] | 21 | 20 |
| Magnet constant | [mT/A] | 1.78 | 4.44 |
| Inductance | [H] | 4.56 | 28.0 |
| 5 G line (r × z) | [m × m] | 3.0 × 3.7 | 3.5 × 4.1 |
| Field homogeneity over the 40 cm DSV, peak-to-peak | [ppm] | 93.5 | 88.1 |

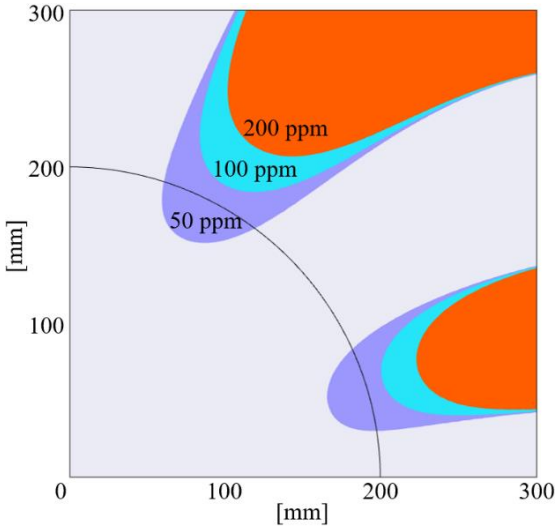


Fig. 4. Homogeneity contour lines near DSV for the 1.5 T MRI magnet.

Additionally, two other MRI magnet designs were included for reliability comparison [27, 28]. We plotted the costs of these four magnets against the magnetic flux passing through their bores in Fig. 6.

We faced two challenges in our cost comparison analysis. First, there were not many published papers that explicitly showed both the manufacturer of the REBCO tape and the total length they used in the design. Second,

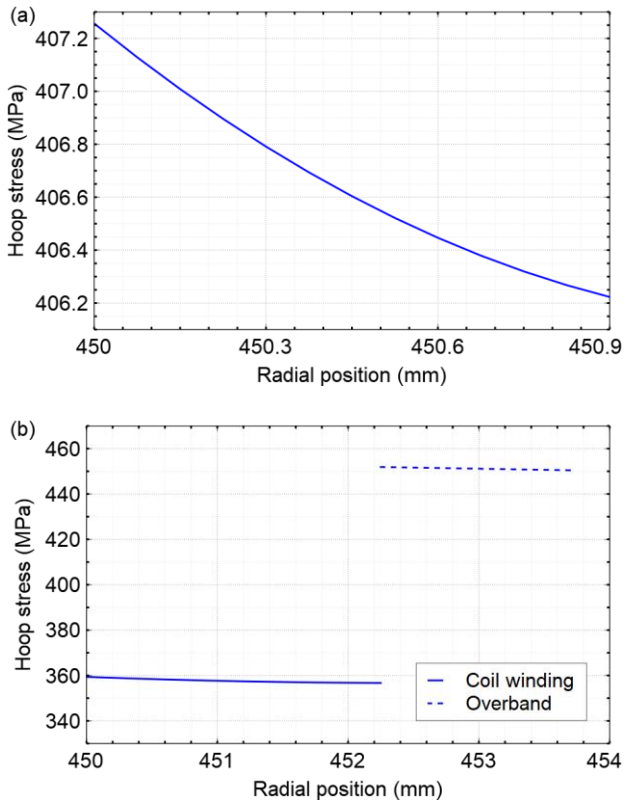


Fig. 5. Magnetic hoop stress of the (a) 1.5 T MRI magnet and the (b) 3.0 T MRI magnet.

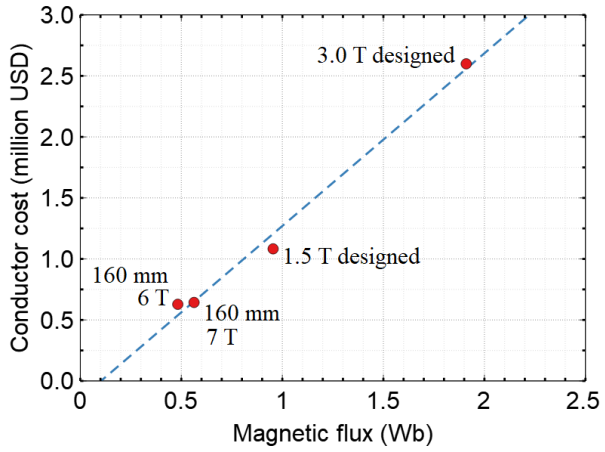


Fig. 6. Conductor cost comparison of the MRI magnet designs with two reference magnets whose inner winding radii are 160 mm.

obtaining price inquiries from manufacturers our institution was not intending to purchase from was difficult. Despite these challenges, we obtained conductor prices from the manufacturers used in the designs through price inquiries [29, 30].

To highlight the relationship, we fitted a linear graph to the data, demonstrating its near-linearity. The largest cost deviation from the linear fitting function was observed in the magnet design [28], with an error of 16.8%.

## 4. CONCLUSION

This paper presents a comparative study of two whole-body MRI magnets, one operating at 1.5 T and the other at 3.0 T. The homogeneity optimization was achieved using a discretized solenoid topology with multi-width winding and outer notches. Both MRI magnets featured a winding inner radius of 450 mm.

For the 1.5 T and 3.0 T MRI designs, the field homogeneities over a 40 cm diameter spherical volume (DSV) were measured at 93.5 ppm and 88.1 ppm, respectively. The conductor usage was calculated at 19.2 km for the 1.5 T magnet and 46.1 km for the 3.0 T magnet. Additionally, both designs achieved fully compressive radial stress and hoop stress below 500 MPa.

The 3.0 T MRI magnet required a 1.5 mm stainless steel overband to reduce hoop stress, while the 1.5 T magnet did not require additional structural support. To provide a comprehensive cost comparison, the designed MRI magnets were analyzed alongside two reference magnets, and the data was represented in a graph with linear fitting. The largest cost deviation from the fitted graph was 16.8%.

## ACKNOWLEDGMENT

This work was supported in part by National R&D Program through the National Research Foundation of Korea(NRF) funded by Ministry of Science and ICT(2022M3I9A1072846), by the Korea Medical Device Development Fund grant funded by the Korea government (the Ministry of Science and ICT, the Ministry of Trade, Industry, and Energy, the Ministry of Health & Welfare, the Ministry of Food and Drug Safety) (Project Number: RS-2020-KD000063), and by the Applied Superconductivity Center, Electric Power Research Institute of Seoul National University.

## REFERENCES

[1] J. Bednorz and K. Müller, "Possible high $T_c$ superconductivity in the Ba−La−Cu−O system," *Z. Phys. B.*, vol. 64, no. 2, pp. 189-193, 1986.

[2] M. Wu, J. Ashburn, C. Torng, P. Hor, R. Meng, L. Gao, Z. Huang, Y. Wang, and C. Chu, "Superconductivity at 93 K in a new mixed-phase Y-Ba-Cu-O compound system at ambient pressure," *Phys. Rev. Lett.*, vol. 58, no. 9, pp. 908-910, 1987.

[3] A. Schilling, M. Cantoni, J. Guo, and H. Ott, "Superconductivity above 130 k in the hg–ba–ca–cu–o system," *Nature*, vol. 363, no. 6424, pp. 56-58, 1993.

[4] T. Baig, Z. Yao, D. Doll, M. Tomsic, and M. Martens, "Conduction cooled magnet design for 1.5 T, 3.0 T and 7.0 T MRI systems," *Supercond. Sci. Technol.*, vol. 27, no. 12, pp. 125012, 2014.

[5] M. Parizh, Y. Lvovsky, and M. Sumption, "Conductors for commercial MRI magnets beyond NbTi: requirements and challenges," *Supercond. Sci. Technol.*, vol. 30, no. 1, pp. 014007, 2016.

[6] A. Malozemoff, W. Carter, S. Fleshler, L. Fritzemeier, Q. Li, L. Masur, P. Miles, D. Parker, R. Parrella, E. Podtburg, G. Riley, M. Rupich, J. Scudiere, and W. Zhang, "HTS wire at commercial performance levels," *IEEE Trans. Appl. Supercond.*, vol. 9, no. 2, pp. 2469-2473, 1999.

[7] A. Malozemoff, D. Verebelyi, S. Fleshler, D. Aized, and D. Yu, "HTS Wire: status and prospects," *Phys. C: Supercond.*, vol. 386, pp. 424-430, 2003.

[8] V. Matias and R. Hammond, "HTS superconductor wire: $5/kAm by 2030," *International Workshop on Coated Conductors for Applications*, 2014.

[9] H. Miura, T. Matsuda, K. Nomura, T. Inoue, Y. Morita, R. Eguchi, S. Otake, H. Tanabe, S. Yokoyama, and S. Sato, "Development of a Half-Size 3 T REBCO Superconducting Magnet for MRI," *J. Phys. Conf. Ser.*, vol. 1559, no. 1, pp. 012125, 2020.

[10] B. Parkinson, R. Slade, M. Mallett, and V. Chamritski, "Development of a cryogen free 1.5 T YBCO HTS magnet for MRI," *IEEE Trans. Appl. Supercond.*, vol. 23, no. 3, pp. 4400405, 2012.

[11] R. Slade, B. Parkinson, and R. Walsh, "Test results for a 1.5 T MRI system utilizing a cryogen-free YBCO magnet," *IEEE Trans. Appl. Supercond.*, vol. 24, no. 3, pp. 4400705, 2013.

[12] D. Gogola, P. Szomolanyi, M. Škrátek, and I. Frollo, "Design and construction of novel instrumentation for low-field MR tomography," *Meas. Sci. Rev.*, vol. 18, no. 3, pp. 107, 2018.

[13] K. Tsuchiya, A. Kikuchi, A. Terashima, K. Norimoto, M. Uchida, M. Tawada, M. Masuzawa, N. Ohuchi, X. Wang, T. Takao, and S. Fujita, "Critical current measurement of commercial REBCO conductors at 4.2 K," *Cryogenics*, vol. 85, pp. 1-7, 2017.

[14] T. Cosmus and M. Parizh, "Advances in whole-body MRI magnets," *IEEE Trans. Appl. Supercond.*, vol. 21, no. 3, pp. 2104-2109, 2010.

[15] L. Wald, P. McDaniel, T. Witzel, J. Stockmann, and C. Cooley, "Low-cost and portable MRI," *J. Magn. Reson. Imaging*, vol. 52, no. 3, pp. 686-696, 2020.

[16] S. Hahn, Y. Kim, D. Park, K. Kim, J. Voccio, J. Bascuñán, and Y. Iwasa, "No-insulation multi-width winding technique for high temperature superconducting magnet," *Appl. Phys. Lett.*, vol. 103, no. 17, pp. 173511, 2013.

[17] L. Hanson, L. Sperling, G. Gard, S. Ipsen, and C. Vergara, "Swedish anthropometrics for product and workplace design," *Appl. Ergon.*, vol. 40, no. 4, pp. 797-806, 2009.

[18] G. Morrow, "Progress in MRI magnets," *IEEE Trans. Appl. Supercond.*, vol. 10, no. 1, pp. 744-751, 2000.

[19] M. McDowell, C. Fryar, and C. Ogden, "Anthropometric reference data for children and adults: United States, 1988-1994," *Vital Health Stat.*, vol. 11, no. 249, pp. 1-68, 2009.
[20] M. Blasche and D. Fischer, "Magnet homogeneity and shimming," *Siemens Healthineers*, 2017.
[21] Mito Toshiyuki, "Development of 1 MJ conduction-cooled LTS pulse coil for UPS-SMES," *IEEE Trans. Appl. Supercond.*, vol. 17, vol. 2, pp. 1973-1976, 2007.
[22] H. Shin and Z. Bautista, "Establishing a test procedure for evaluating the electromechanical properties of practical REBCO coated conductor tapes by the uniaxial tension test at 77 K," *Supercond. Sci. Technol.*, vol. 32, no. 6, pp. 064004, 2019.
[23] P. Gao, J. Mao, J. Chen, X. Wang, and Y. Zhou, "Electromechanical degradation of REBCO coated conductor tapes under combined tension and torsion loading," *Int. J. Mech. Sci.*, vol. 223, pp. 107314, 2022.
[24] H. Shin and Z. Bautista, "Evaluation of irreversible strain/stress limits for Ic degradation in practical REBCO CC tapes under uniaxial tension," *IEEE Trans. Appl. Supercond.*, vol. 28, no. 4, pp. 8400305, 2017.
[25] K. Kim, K. Bhattarai, K. Kim, H. Bai, I. Dixon, T. Painter, U. Bong, D. Larbalestier, and S. Hahn, "Design and performance estimation of a 20 T 46 mm no-insulation all-REBCO user magnet," *IEEE Trans. Appl. Supercond.* vol. 30, no. 4, pp. 4602205, 2020.
[26] Y. Iwasa, *Case studies in superconducting magnets: design and operational issues*, 2nd ed., Springer science & business media, pp. 98-99, 2009.
[27] W. Jang, G. Kim, K. Choi, J. Park, J. Bang, and S. Hahn, "Electromagnetic design study of a 7 T 320 mm high-temperature superconducting MRI magnet with multi-width technique incorporated," *Prog. Supercond. Cryog.*, vol. 23, no. 4, pp. 30-34, 2021.
[28] K. Choi, J. Bang, C. Lee, J. Kim, B. Eom, S. Kim, G. Kim, C. Im, J. Kim, H. Noh, Y. Hwang, M. Sohn, M. Ahn, S. Kim, H. Lee, K. Sim, and S. Hahn, "Design of a cryogen-free 6 T 320 mm all-REBCO MRI magnet," *International Conference on Magnet Technology*, 2021.
[29] SuNAM, 2023.
[30] SuperOx, 2023.